

The effect of H₂O on the olivine liquidus of basaltic melts: experiments and thermodynamic models

Etienne Médard · Timothy L. Grove

Received: 3 May 2007 / Accepted: 3 September 2007 / Published online: 9 October 2007
© Springer-Verlag 2007

Abstract We designed and carried out experiments to investigate the effect of H₂O on the liquidus temperature of olivine-saturated primitive melts. The effect of H₂O was isolated from other influences by experimentally determining the liquidus temperatures of the same melt composition with various amounts of H₂O added. Experimental data indicate that the effect of H₂O does not depend on pressure or melt composition in the basaltic compositional range. The influence of H₂O on melting point lowering can be described as a polynomial function $\left(C_{\text{H}_2\text{O}}^{\text{melt}} \text{ in wt\%}\right) : \Delta T \text{ (}^\circ\text{C)} = 40.4\left(C_{\text{H}_2\text{O}}^{\text{melt}}\right) - 2.97\left(C_{\text{H}_2\text{O}}^{\text{melt}}\right)^2 + 0.0761\left(C_{\text{H}_2\text{O}}^{\text{melt}}\right)^3$. This expression can be used to account for the effect of H₂O on olivine-melt thermometers, and can be incorporated into fractionation models for primitive basalts. The non-linear effect of H₂O indicates that incorporation of H₂O in silicate melts is non-ideal, and involves interaction between H₂O and other melt components. The simple speciation approach that seems to account for the influence of H₂O in simple systems (albite-H₂O, diopside-H₂O) fails to describe the mixing behavior of H₂O in multi-component silicate melts. However, a non-ideal solution model that treats the effect of H₂O addition as a positive excess free energy can be fitted to describe the effect of melting point lowering.

Introduction

It has long been understood that water plays an important role in magmatic processes. Water has a large effect on the mantle solidus (Mysen and Boettcher 1975; Grove et al. 2006) and is responsible for the initiation of melting in subduction zones, as well as broadening of the melting zone under mid-ocean ridges (Asimow and Langmuir 2003). Water also drastically changes the liquid line of descent of basaltic magmas: it is responsible for the calcalkaline versus tholeiitic differentiation trend (Grove and Baker 1984), and small amount of H₂O have been argued to have an important effect on the crystallization of mid-ocean ridges magmas (Michael and Chase 1987). Significant water contents have been inferred from primitive magmas in subduction-zone settings (e.g., Anderson 1979; Sisson and Grove 1993b; Sisson and Layne 1993; Sobolev and Chaussidon 1996), back-arc basins (Danyushevsky et al. 1993; Stolper and Newman 1994), intraplate settings (Dixon et al. 1997; Spilliaert et al. 2006), and even at some mid-ocean ridges (Danyushevsky 2001).

However, even if the qualitative effect of water on magmatic processes has been long understood, quantitative estimates are scarce and often incompatible with each other. This is a consequence of the experimental difficulties inherent in carrying out hydrous experiments, including the ability to maintain a constant H₂O content, and to quench water-rich hydrous melts to analyzable glasses. For example, empirical and thermodynamic models of the effect of water on the olivine-melt equilibrium show a very large variability (Fig. 1; Ghiorso and Sack 1995; Falloon and Danyushevsky 2000; Sugawara 2000; Ghiorso et al. 2002; Ariskin and Barmina 2004). The olivine-melt equilibrium is of critical importance for the understanding of

Communicated by J. Hoefs.

E. Médard (✉) · T. L. Grove
Department of Earth, Atmospheric, and Planetary Sciences,
Massachusetts Institute of Technology,
77 Massachusetts Avenue, Building 54-1212,
Cambridge, MA 02139, USA
e-mail: etienne.medard@erdw.ethz.ch

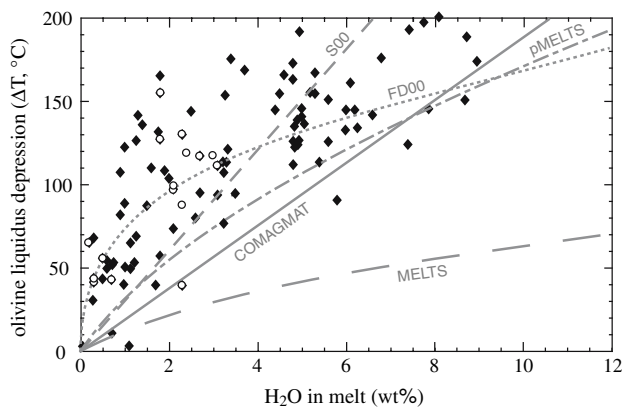


Fig. 1 Calculated olivine liquidus depression as a function of H₂O content in the melt, updated from Falloon and Danyushevsky (2000). Liquidus depression is calculated as the difference between experimental temperature and a hypothetical dry liquidus temperature calculated from the Ford et al. (1983) geothermometer. This thermometer was used because it gave the best agreement between predicted and measured temperatures for dry experiments on 82–72f composition. *Solid symbols* are for basaltic compositions (46–52 wt% SiO₂), circles are the data of Falloon and Danyushevsky (2000, 49–53 wt% SiO₂). Data sources are the ones cited in Falloon and Danyushevsky (2000), as well as more recent data by Pichavant et al. (2002), Laporte et al. (2004), Parman and Grove (2004), Kägi et al. (2005) and Médard et al. (2006). Also plotted are calculated liquidus depressions for basalt 82–72f using the following models: FD00 (Falloon and Danyushevsky 2000), S00 (Sugawara 2000), pMELTS (Ghiorso et al. 2002), MELTS (Ghiorso and Sack 1995) and COMAGMAT (Ariskin and Barmina 2004)

magmatic processes: since olivine is the low-pressure liquidus phase in mantle-derived magmas, thermometry based on the olivine-melt equilibrium provides the primary evidence for estimating melting temperatures in the Earth's mantle (e.g., Roeder and Emslie 1970; Ford et al. 1983; Green et al. 2001; Putirka 2005). Assessing the influence of H₂O is thus critical for the determination of mantle temperatures in subduction zones and ocean islands settings. Quantification of the influence of H₂O on olivine-melt equilibrium is also required for calculating the liquid line of descent of primitive H₂O-bearing magmas (Danyushevsky 2001). Furthermore, since olivine is the dominant phase in the upper mantle, the effect of water on the olivine-melt equilibrium can be used as a first approximation to parameterize hydrous melting models (Langmuir et al. 2006).

This paper presents experiments aimed at quantifying the effect of water on the liquidus of olivine-saturated primitive basaltic and andesitic melts. We also develop a thermodynamic model to understand the effect of water on the olivine-melt equilibrium. Our experimental approach has been to measure the dry liquidus temperature, and liquidus temperatures for various amounts of added H₂O, on the same bulk composition. For each

H₂O concentration, we then calculate the liquidus depression, ΔT , as the difference between the dry liquidus temperature at a given pressure and the liquidus temperature for the same melt composition with a known amount of H₂O added. This method allows us to separate the effect of H₂O from other potential influences (e.g., melt composition, pressure). Previous studies on the melting point lowering effect of H₂O show a large dispersion of data (e.g., Fig. 1). The input data for these models were made on samples of different composition, under conditions of variable f_{O_2} , different pressures, and by comparing measured H₂O-bearing liquidus values with estimates of the dry liquidus. Furthermore, accurate determination of H₂O concentration was not always available.

Here, we determine liquidus temperatures for one melt composition (basalt 82–72f) under anhydrous conditions and at a variety of water contents under a restricted range of oxygen fugacity. Most of the H₂O-bearing experiments were performed under water-saturated conditions and the water contents were analyzed using a variety of methods. We will show that pressure and melt composition have little influence on liquidus depression. The dispersion in Fig. 1 should thus mainly be attributed to the use of calculated dry liquidus temperatures, analytical uncertainties for the H₂O concentration, and/or interlaboratory calibrations.

Experimental and analytical procedures

Starting materials

Experiments have been performed on a primitive high-alumina basalt from the Giant Crater Lava Field, Medicine Lake Volcano, California (sample 82–72f, Donnelly-Nolan et al. 1991; Table 1). This fine grained, equigranular, non-porphyrific, dyktitaxitic basalt is the most primitive lava from Medicine Lake Volcano, and is close in composition to a low-pressure melt of a mantle lherzolite source (Bartels et al. 1991). This composition is also very close to that of a primitive mid-ocean ridge basalt (Table 1), except for higher Al₂O₃ contents. Small rock chips from 82–72f were reduced to homogeneous powders by grinding in a SPEX WC shatterbox, and used as starting material.

A smaller number of experiments have been performed on two other compositions spanning the compositional range of primitive mantle melts, in order to investigate the effect of melt composition on olivine liquidus-depression. Sample 85–41c (Baker et al. 1994; Table 1) is a primitive magnesian andesite from Mount Shasta, California, that may represent the product of fluxed-melting in the mantle

Table 1 Starting compositions (wt%)

	82–72f	140DS1	N-MORB	85–41c	Bb-107
SiO ₂	47.73	49.89	49.54	57.80	46.76
TiO ₂	0.59	1.02	0.90	0.60	1.27
Al ₂ O ₃	18.51	15.59	16.76	14.46	12.40
FeO	8.21	9.46	8.06	5.74	9.10
MnO	0.15	0.17	0.14	0.11	0.15
MgO	10.51	9.51	9.75	9.14	10.49
CaO	12.01	12.04	12.51	8.17	12.03
Na ₂ O	2.16	2.19	2.18	3.11	3.17
K ₂ O	0.07	0.06	0.07	0.71	3.27
P ₂ O ₅	0.06	0.07	0.10	0.15	1.36
NBO/T	0.768	0.819	0.779	0.599	1.241

82–72f is from Donnelly-Nolan et al. (1991); 140DS1 is the basalt used by Almeev et al. (2007); N-MORB is glass average from Workman and Hart (2005); 85–41c from Baker et al. (1994) and Bb-107 is an average of four superliquidus experiments on the synthetic starting material prepared by Holbig and Grove (2007). All analyses renormalized to 100%

wedge (Grove et al. 2005). Composition Bb107 (Turner et al. 1996) is a primitive olivine-leucitite from the Tibetan plateau. Because a natural sample was not available, a synthetic starting material made from analytical grade oxides (Holbig and Grove 2007; Table 1) was used for the olivine-leucitite experiments.

Dry experiments

The dry liquidus for 82–72f, 85–41c, and Bb107 have been determined at atmospheric pressure using one-atmosphere gas mixing furnaces, and at high pressure in a 12.7 mm end-loaded piston-cylinder (Table 2).

The 0.1 MPa liquidus for 82–72f was previously determined by Bartels et al. (1991). For the two other compositions, experiments were performed in a Deltech rapid quench gas-mixing furnace. Oxygen fugacity was controlled at or near the nickel–nickel oxide (NNO) buffer using mixtures of CO₂–H₂, and monitored by CaO–ZrO₂ electrolyte cells. The starting material was pressed into pellets with Elvanol as a binder. The pellets were sintered to a PtFe alloy loop containing 4–6 wt% Fe designed to minimize the exchange of iron between the silicate charge and the wire loop (Grove 1981). Experimental durations varied from 1 h (in order to minimize the Na₂O loss for Bb107) to 4.7 h.

High-pressure experiments have been performed using a 12.7 mm end-loaded solid-medium piston-cylinder device (Boyd and England 1960). The assemblies were prepared by packing ~10 mg of powder into a graphite crucible with a graphite lid. The crucible was then placed in a platinum capsule that had been triple crimped, welded shut and flattened on one end. Graphite powder was packed in above and below the crucible, and the loaded capsule was dried at 400°C overnight in a pot-furnace to ensure anhydrous conditions during the experiment. The top of the outer Pt

Table 2 Dry experiments: summary of experimental conditions and results

Run	P (MPa)	T (°C)	Dur. (h)	Phases ^b	ΔFe ^c	X _{Mg} ol	K _D ^d	K _{Mg} ^d
82–72f								
B994	800	1,320	3.5	liq, ol(tr)	0.001	0.879	0.32	4.42
B988	800	1,310	3.3	liq, ol(1)	0.014	0.871	0.33	4.56
B1043	1,000	1,340	4.0	liq	0.004			
B1042	1,000	1,330	4.0	liq, ol(tr)	–0.006	0.880	0.31	4.45
85–41c								
#13	0.1	1,250	4.7	liq, sp(tr)	0.003			
#14	0.1	1,244	4.5	liq, ol(1), sp(tr)	–0.030	0.914	0.28	5.37
Bb-107								
#9	0.1	1,278	1.0	liq	0.052			
#13	0.1	1,266	4.0	liq, ol(tr)	0.043	0.887	0.25	4.61
B1030	800	1,330	4.2	liq	0.037			
B1054	800	1,320	4.2	liq, ol(2)	0.005	0.869	0.29	4.81
B1051	1,000	1,350	4.0	liq	0.003			
B910 ^a	1,000	1,335	3.0	liq, ol(2)	0.025	0.866	0.29	4.82

^a Experiment from Holbig and Grove (2007)

^b Phase proportions in wt%, tr indicates proportions <0.5 wt%

^c Relative loss (–) or gain (+) of FeO during the experiment

^d Partition coefficients between olivine and melt: $K_{Mg} = (MgO_{olivine})/(MgO_{melt})$, $K_{Fe} = (FeO_{olivine})/(FeO_{melt})$, $K_D = K_{Fe}/K_{Mg}$

capsule was then crimped and welded shut. The capsule was fitted in an alumina sleeve and positioned in the hotspot of a straight-walled graphite furnace using MgO spacers. The pressure medium consisted of sintered BaCO₃, which has been found to have no friction correction through calibration against the reaction Ca-Tschermak pyroxene = anorthite + gehlenite + corundum (Hays 1966). Pressures are thought to be accurate to within ±0.05 GPa. The temperature was monitored and controlled using W₉₇Re₃–W₇₅Re₂₅ thermocouples, with no correction for the effect of pressure on thermocouple emf and was controlled to within ±2°C of the setpoint using a Eurotherm controller. Temperatures are thought to be accurate to ±10°C. The thermocouple was positioned above the sample in the cooler upper part of the furnace; a correction of +20°C was added to the thermocouple temperature. This temperature difference has been independently determined using two different techniques: direct measurement with offset thermocouples, and temperature mapping using the kinetics of the MgO + Al₂O₃ = MgAl₂O₄ reaction (Watson et al. 2002). Experiments were pressurized at room temperature, after which the temperature was raised to 865°C at 100°C/min, held constant for 6 min, and increased at a rate of 50 °C/min to the desired experimental conditions. The experiments were terminated by shutting off the power to the apparatus. Experimental conditions and results for dry experiments are presented in Table 2.

Water-bearing experiments

H₂O-saturated experiments have been performed between 10 and 200 MPa in a MHC (Molybdenum Hafnium Carbide) cold-seal pressure vessel using Au₈₀Pd₂₀ outer capsules and Au₉₀Pd₁₀ or Au₈₀Pd₂₀ inner capsules, depending on the temperature (Table 3). Oxygen fugacity was buffered by a solid Ni–NiO assemblage contained in Pt capsules. Inner capsule and buffer capsules were crimped closed, but not welded, to ensure that the oxygen buffer and the sample were in contact with the same fluid phase. Details of the experimental procedure are presented in Sisson and Grove (1993a). Reported experimental temperatures are precise to ±7°C, and pressures to ±0.5 MPa. The difference between thermocouple temperature and sample temperature was frequently checked during the course of the experimental study. Most of the inner capsules were preconditioned to avoid Fe-loss during the experiment. Au₈₀Pd₂₀ capsules were filled with 82–72f powder and placed in a 1 atm furnace at log fO₂ = QFM and 1,250°C for 72 h. The melting point of Au₉₀Pd₁₀ is well below the dry liquidus for 82–72f, so Au₉₀Pd₁₀ capsules were filled with either a basaltic andesite powder (85–44, Baker et al. 1994) for experiments with 82–72f or

Bb107, or with 85–41c powder for 85–41c experiments, and reacted at log fO₂ = QFM and 1,170°C for 72 h. The silicate glass was then removed in a hot HF + HNO₃ bath. The conditions and results of each experiment are given in Table 3. Most experiments were synthesis experiments, where temperature was increased to the target temperature and held constant for 1–4 h. Two reversal experiments (82–72f#13 and 82–72f#18) were performed at 200 MPa by heating 20–30°C above the target temperature for 30 min to completely melt the starting material, and then dropping the temperature. Short run durations were required to avoid H₂O-loss from the experiments. At the end of an experiment, the capsules were drilled under a stereomicroscope to check for water saturation. Experiments at the lower pressures investigated (10 and 25 MPa) were not water-saturated, probably as a consequence of water-loss through the capsule walls due to high temperatures and low initial water-content. However, in these experiments, H₂O concentrations are homogeneous throughout the entire experimental glasses.

Two water-saturated experiments were performed at 1.0 GPa, using a trash-can setup in a 12.7 mm end-loaded solid-medium piston-cylinder device. The outer Au₈₀Pd₂₀ capsule was triple-crimped and welded shut on one end, and the other end was flattened out to obtain a flat horizontal rind around the rim of the capsule. A pre-conditioned inner Au₉₀Pd₁₀ capsule was filled with ~10 mg of the starting material and placed inside the Au₈₀Pd₂₀ capsule together with a Pt capsule filled with a Ni–NiO buffer and ~25 µL of distilled water, a setup similar to that of the MHC experiments. The outer capsule was then fitted into a pyrophyllite sleeve and covered with a flat Au₈₀Pd₂₀ lid. The rest of the assembly, and the experimental procedure were identical to those used for the dry experiments. The outer capsule sealed successfully during the pressurization of the experiments, and samples were still water-saturated after a 5 h run.

Two water-undersaturated experiments were also performed at 1.0 GPa, using a mix of 82–72f powder and hydrous glass from water-saturated experiment 82–72f#1. The experimental setup was identical to the one used for dry experiments, except for a pyrophyllite sleeve replacing the alumina sleeve around the Pt capsule.

Analytical techniques

After each experiment, the entire sample was extracted from the capsule, broken down into small transparent pieces in an agate mortar, and examined under an optical microscope to check for the presence of olivine crystals. In the glassy material, even a single olivine crystal was easy to spot due to its high birefringence. All the olivine crystals

Table 3 Hydrous experiments: summary of experimental conditions and results

Run	<i>P</i> (MPa)	<i>T</i> (°C)	Caps. ^a	Dur. (h)	Phases ^b	ΔFe^c	Sat. ^d	H_2O concentration (wt%) ^e				$X_{\text{Mg ol}}$	K_{D}^f	K_{Mg}^f	ΔT^g
								SIMS	Oxy.	Diff.	Sol.				
82–72f															
#19	10	1,230	sAu ₈₀	2.1	liq	0.043		0.44(8)	1.1(5)	1.1(4)	0.84				38
#23	10	1,220	sAu ₈₀	1.5	liq, ol(1)	–0.001		0.67(10)	0.3(4)	0.8(4)	0.84	0.881	0.30	4.61	48
#10	25	1,213	sAu ₈₀	2.0	liq	0.042		1.39(13)	1.5(3)	1.5(4)	1.45				56
#11	25	1,204	sAu ₈₀	2.0	liq, ol(tr)	0.004		1.00(4)	1.0(3)	1.3(4)	1.46	0.881	0.30	4.58	65
#9	50	1,199	Au ₉₀	2.0	liq	–0.098	Yes	2.28(13)	2.3(4)	2.4(6)	2.18				71
#8	50	1,190	Au ₉₀	3.1	liq, ol(tr)	–0.127	Yes		2.3(3)	2.2(5)	2.19	0.899	0.30	4.57	80
#6	100	1,189	Au ₉₀	2.3	liq	–0.123	Yes		3.4(4)	3.1(4)	3.24				84
#7	100	1,173	Au ₉₀	2.0	liq, ol(1)	–0.054	Yes	3.0(3)	3.4(4)	3.3(6)	3.26	0.895	0.29	4.51	100
#1	200	1,210	sAu ₈₀	3.1	liq	–0.068	Yes		4.8(5)	4.6(6)	4.66				70
#12	198	1,170	Au ₉₀	3.1	liq	–0.085	Yes	4.4(3)			4.69				110
#4	200	1,159	Au ₉₀	2.1	liq	–0.055	Yes		5.1(5)	4.7(5)	4.74				121
#18	198	1,157	sAu ₉₀	2.4	liq	–0.016	Yes	4.4(2)	4.5(6)	4.6(7)	4.72				123
#13	200	1,147	sAu ₉₀	2.5	liq, ol(1)	–0.060	Yes	4.9(3)	4.6(5)	4.7(5)	4.76	0.891	0.30	4.51	133
#5	200	1,144	Au ₉₀	2.5	liq, ol(1)	–0.079	Yes		5.0(5)	5.2(5)	4.76	0.885	0.33	4.49	136
B1084	1,000	1,160	sAu ₉₀	4.0	liq	0.022	Yes				11.5				172
B1081	1,000	1,140	sAu ₉₀	5.0	liq, ol	0.007	Yes				11.5	0.880	0.30	4.63	192
B1065	1,000	1,305	Pt-C	2.0	liq, ol(1)	–0.006		0.61(5)				0.880	0.31	4.59	27
B1064	1,000	1,300	Pt-C	2.0	liq, ol(tr)	–0.028		0.78(4)				0.884	0.31	4.52	32
85–41c															
#128	197	1,160	sAu ₉₀	2.4	liq, sp(tr)	–0.034	Yes		6.2(6)	5.6(6)	5.11				101
#127	198	1,150	sAu ₉₀	3.3	liq, ol(tr), sp(tr)	–0.024	Yes	6.2(5)	5.7(6)	6.0(6)	5.14	0.909	0.29	5.42	111
#126	198	1,130	sAu ₉₀	2.3	liq, ol(3), sp(tr)	–0.047	Yes		6.5(6)	5.5(6)	5.12	0.904	0.29	6.05	131
Bb-107															
#4	200	1,179	sAu ₉₀	1.3	liq	–0.018	Yes	5.2(4)	4.8(5)	4.5(5)	5.11				109
#3	199	1,170	sAu ₉₀	2.5	liq	0.010	Yes		4.7(5)	4.1(5)	5.11				118
#1	200	1,147	sAu ₉₀	2.6	liq, ol(1)	–0.015	Yes		5.5(6)	4.8(5)	5.17	0.874	0.30	4.59	141

^a Capsules are made of Au₉₀Pd₁₀ or Au₈₀Pd₂₀, s indicate that the capsule has been preconditioned to avoid iron loss

^b Phase proportions in wt%, tr indicates proportions <0.5 wt%

^c Relative loss (–) or gain (+) of Fe during the experiment

^d Indicate if the capsules contained free water at the end of the experiment, i.e. if they were water-saturated

^e H₂O concentrations have been analyzed by SIMS, and determined from oxygen (oxy.) analyses and from analytical totals (diff.) with the EMP. sol. is the solubility calculated with the Moore et al. (1998) model. The numbers in parentheses are uncertainties given in terms of the last unit cited, thus 6.2(5) should be read 6.2 ± 0.5. Uncertainties are a combination of 1σ standard deviations of the analyses and propagated errors on the calibration curves

^f Partition coefficients between olivine and melt: $K_{\text{Mg}} = (\text{MgO}_{\text{olivine}})/(\text{MgO}_{\text{melt}})$, $K_{\text{Fe}} = (\text{FeO}_{\text{olivine}})/(\text{FeO}_{\text{melt}})$, $K_{\text{D}} = K_{\text{Fe}}/K_{\text{Mg}}$ (melt components calculated on an anhydrous basis)

^g ΔT is the difference between the dry liquidus and the experimental temperature, in °C

show euhedral equilibrium shapes. Experimental charges were then analyzed with the JEOL 733 electron microprobes at the Massachusetts Institute of Technology. A 10 nA beam current and 15 kV accelerating potential were used for all analyses. Beam diameter was set to 2 μm for olivine, and 20 μm for glasses. On-line data reduction was accomplished using the CITZAF correction package (Armstrong 1995). Analytical precision is estimated from replicate analyses of a basalt glass working standard, and standard deviations are: 1.08% for SiO₂, 1.26% for Al₂O₃,

1.31% for CaO, 1.67% for MgO, 2.4% for FeO, 3.5% for K₂O, 8.7% for TiO₂, 9.2% for Na₂O, 12% for P₂O₅, 22% for MnO and 67% for Cr₂O₃. Analytical results are presented in Table 4.

H₂O concentrations of selected experimental glasses were determined using the Cameca IMS-3f ion microprobe at Woods Hole Oceanographic Institution (Table 3). Samples were mounted in epoxy (H₂O content ≥1.5 wt%) or indium (H₂O content ≤1.5 wt%), left to degas overnight at 60°C under vacuum to reduce adsorbed H₂O, and

Table 4 Electron microprobe analyses of run products (wt%)

Run	Phase	<i>n</i>	SiO ₂	TiO ₂	Al ₂ O ₃	FeO	MnO	MgO	CaO	Na ₂ O	K ₂ O	P ₂ O ₅	NiO	Total
82–72f														
B994	liq	7	47.64(15)	0.59(7)	18.67(6)	8.22(13)	0.14(2)	10.71(9)	11.61(10)	2.28(15)	0.08(2)	0.06(2)		99.62
	ol	6	40.0(3)	0.02(2)	0.09(2)	11.6(2)	0.15(3)	47.1(3)	0.35(3)				0.12(1)	99.45
B988	liq	6	47.73(12)	0.61(8)	18.89(8)	8.29(25)	0.15(2)	10.20(10)	11.76(7)	2.26(12)	0.08(2)	0.04(3)		99.65
	ol	6	40.1(3)	0.03(2)	0.10(4)	12.2(2)	0.15(2)	46.2(3)	0.37(8)				0.10(2)	99.34
B1043	liq	6	47.7(2)	0.69(9)	18.41(5)	8.24(8)	0.14(2)	10.57(23)	11.76(5)	2.33(7)	0.09(3)	0.05(2)		99.65
B1042	liq	5	47.90(6)	0.66(9)	18.47(13)	8.16(8)	0.13(2)	10.52(9)	11.74(7)	2.28(8)	0.08(3)	0.03(2)		99.46
	ol	6	40.9(3)	0.03(2)	0.12(2)	11.35(11)	0.19(3)	46.72(28)	0.37(2)				0.05(1)	99.76
#19	liq	20	47.3(5)	0.57(6)	18.6(2)	8.57(3)	0.15(2)	10.6(2)	11.73(13)	2.24(11)	0.07(3)	0.06(2)		98.05
#23	liq	7	48.1(2)	0.54(6)	18.61(19)	8.2(2)	0.13(2)	10.22(9)	11.83(10)	2.22(18)	0.08(3)	0.08(2)		99.13
	ol	7	41.1(4)	0.02(2)	0.06(2)	11.5(5)	0.16(3)	47.6(3)	0.37(2)				0.23(2)	101.14
#10	liq	20	47.6(3)	0.53(6)	18.48(13)	8.55(23)	0.16(3)	10.64(10)	11.63(15)	2.21(11)	0.08(3)	0.06(2)		98.08
#11	liq	20	47.9(4)	0.54(8)	18.66(13)	8.24(33)	0.14(3)	10.41(16)	11.68(15)	2.03(15)	0.08(3)	0.04(2)		98.29
	ol	7	39.9(2)	0.03(2)	0.04(2)	11.4(3)	0.19(4)	47.7(4)	0.38(3)				0.20(4)	99.89
#9	liq	20	48.3(1)	0.56(9)	18.70(12)	7.41(13)	0.15(3)	10.73(10)	11.73(15)	2.30(14)	0.07(3)	0.06(2)		97.18
#8	liq	19	48.4(4)	0.59(7)	18.79(9)	7.16(15)	0.16(3)	10.61(14)	11.76(13)	2.25(13)	0.09(3)	0.04(2)		97.09
	ol	8	40.6(5)		0.08(4)	9.8(7)	0.17(3)	48.5(8)	0.37(3)				0.43(9)	99.93
#6	liq	17	48.2(3)	0.58(5)	18.75(11)	7.20(12)	0.15(3)	10.87(19)	11.77(16)	2.32(10)	0.09(3)	0.06(2)		95.55
#7	liq	20	48.0(2)	0.58(7)	18.68(10)	7.77(14)	0.16(3)	10.73(14)	11.70(12)	2.29(12)	0.08(3)	0.05(2)		95.43
	ol	9	40.9(5)	0.02(2)	0.08(2)	10.1(3)	0.16(3)	48.4(6)	0.37(4)				0.18(4)	100.56
#1	liq	10	48.05(14)	0.64(4)	18.64(15)	7.6(2)	0.17(2)	10.67(5)	11.70(10)	2.3(2)	0.07(2)	0.06(3)		93.81
#12	liq	10	47.6(2)	0.57(7)	19.30(17)	7.51(10)	0.11(2)	10.60(9)	11.93(9)	2.21(9)	0.07(3)	0.05(2)		94.52
#4	liq	17	47.6(4)	0.65(9)	18.83(14)	7.76(15)	0.16(3)	10.80(8)	11.71(11)	2.30(11)	0.08(3)	0.04(3)		93.73
#18	liq	11	47.5(3)	0.56(7)	18.68(12)	8.08(8)	0.15(3)	10.84(20)	11.75(16)	2.31(17)	0.08(3)	0.06(2)		93.89
#13	liq	14	48.0(5)	0.59(9)	18.72(16)	7.72(24)	0.17(6)	10.68(13)	11.64(24)	2.32(14)	0.08(3)	0.03(3)		93.75
	ol	6	40.4(3)	0.04(2)	0.09(2)	10.5(3)	0.21(2)	48.0(4)	0.31(4)				0.16(6)	99.79
#5	liq	15	48.2(2)	0.59(7)	18.72(13)	7.56(9)	0.15(4)	10.67(10)	11.68(8)	2.24(13)	0.08(3)	0.06(3)		93.87
	ol	11	40.0(3)		0.05(2)	11.0(5)	0.18(3)	47.8(6)	0.30(5)				0.22(4)	99.64
B1084	liq	11	48.5(6)	0.60(8)	18.5(2)	8.4(2)	0.16(2)	10.8(4)	12.1(7)	0.9(2) ^a	0.04(2)	0.04(3)		81.96 ^a
B1081	liq	9	47.9(6)	0.44(7)	19.2(4)	8.3(4)	0.15(2)	10.2(4)	12.4(6)	1.3(2) ^a	0.08(2)	0.06(2)		80.82 ^a
	ol	7	40.4(3)		0.06(3)	11.4(3)	0.18(3)	46.8(3)	0.32(4)				0.23(3)	99.43
B1065	liq	11	47.6(3)	0.59(6)	18.8(2)	8.16(11)	0.17(3)	10.32(10)	11.9(2)	2.31(14)	0.08(2)	0.07(2)		98.86
	ol	6	40.0(3)	0.02(2)	0.10(2)	11.5(3)	0.12(2)	47.1(2)	0.34(2)				0.14(4)	99.31
B1064	liq	11	47.9(2)	0.57(6)	18.67(8)	7.98(12)	0.15(3)	10.6(3)	11.8(2)	2.19(12)	0.07(3)	0.04(2)		98.76
	ol	7	40.1(2)		0.11(3)	11.1(4)	0.14(3)	47.5(4)	0.36(2)					99.33
85–41c														
#13	liq	6	58.1(3)	0.56(6)	14.43(13)	5.76(8)	0.14(3)	9.09(12)	7.9(3)	3.21(6)	0.68(9)	0.12(2)		100.44
#14	liq	6	58.1(2)	0.63(8)	14.41(8)	5.57(14)	0.11(2)	9.26(7)	8.08(12)	3.04(7)	0.65(3)	0.10(3)		99.41
	ol	16	41.2(3)	0.02(1)	0.03(2)	8.34(14)	0.12(2)	49.8(2)	0.22(2)				0.24(3)	100.07
#128	liq	16	57.9(4)	0.57(6)	14.8(2)	5.55(9)	0.09(4)	9.07(12)	8.13(13)	3.07(15)	0.67(3)	0.13(4)		94.22
#127	liq	25	57.7(3)	0.56(7)	14.8(2)	5.59(14)	0.10(4)	9.17(13)	8.23(12)	3.06(17)	0.66(3)	0.14(4)		94.04
	ol	9	41.0(4)	0.01(1)	0.03(1)	8.9(3)	0.16(3)	49.8(4)	0.19(2)				0.04(5)	100.25
#126	liq	12	58.5(4)	0.56(7)	15.1(3)	5.37(16)	0.08(3)	8.16(15)	8.36(15)	3.07(13)	0.68(3)	0.12(4)		94.62
	ol	7	40.8(2)	0.02(1)	0.01(1)	9.4(3)	0.14(2)	49.2(2)	0.18(1)				0.08(5)	99.86
Bb107														
#9	liq	5	46.4(6)	1.25(5)	12.3(1)	9.6(5)	0.15(3)	10.6(2)	12.1(2)	3.14(16)	3.20(10)	1.36(10)		99.52
#13	liq	6	47.3(2)	1.24(7)	12.54(5)	9.48(7)	0.14(2)	10.34(15)	12.02(18)	2.68(13)	2.99(3)	1.20(11)		99.94
	ol	7	40.5(2)	0.03(1)	0.06(1)	10.76(13)	0.15(3)	47.5(2)	0.64(3)					99.68

Table 4 continued

Run	Phase	<i>n</i>	SiO ₂	TiO ₂	Al ₂ O ₃	FeO	MnO	MgO	CaO	Na ₂ O	K ₂ O	P ₂ O ₅	NiO	Total
B1030	liq	10	46.5(3)	1.23(7)	12.29(13)	9.35(15)	0.14(2)	10.50(13)	12.22(16)	3.27(14)	3.21(14)	1.27(11)		98.62
B1054	liq	7	47.1(2)	1.19(6)	12.52(12)	9.1(2)	0.13(2)	9.74(13)	12.30(13)	3.33(13)	3.27(5)	1.33(5)		99.88
	ol	6	40.04(8)	0.02(1)	0.05(1)	12.6(2)	0.18(2)	47.18(16)	0.57(3)					100.66
B1051	liq	9	46.7(3)	1.24(9)	12.32(9)	9.05(10)	0.13(3)	10.54(12)	12.06(13)	3.25(16)	3.33(6)	1.32(6)		99.69
#4	liq	10	47.0(3)	1.32(6)	12.41(6)	8.87(18)	0.17(2)	10.44(15)	11.90(8)	3.06(10)	3.28(10)	1.55(10)		93.92
#3	liq	14	46.7(2)	1.27(9)	12.58(15)	9.12(6)	0.15(3)	10.46(11)	11.95(11)	3.08(13)	3.27(7)	1.37(7)		94.37
#1	liq	9	47.0(4)	1.19(9)	12.61(7)	8.93(8)	0.16(2)	10.24(12)	11.98(21)	3.18(12)	3.24(11)	1.43(11)		94.18
	ol	13	40.4(3)	0.04(1)	0.01(1)	12.2(6)	0.19(3)	47.1(4)	0.46(2)					100.39

The numbers in parentheses are 1σ standard deviations, given in terms of the last unit cited, thus 8.16(8) should be read 8.16 ± 0.08 . Glass compositions have been renormalized to 100% anhydrous, original totals are reported in the last column

n is the number of analyses per phase. All Fe is reported as FeO

^a The melt quenched to a fine-grained mix of glass, crystals and bubbles that has been analyzed with a 30 μm defocused beam. Na₂O concentrations are low due to Na diffusion during analyses of the H₂O-rich “glasses”

sputter-coated with 30 nm of Au. The primary ¹⁶O[−] ion beam, accelerated through 8 keV, was focused on the sample to a spot with a diameter of 8–12 μm that was centered in the 150 μm diameter area imaged by the secondary ion optics. The areas of glass to be analyzed were cleaned of Au and surface contamination by rastering the primary beam over a square area slightly greater than 50 μm on a side for 5 min. Following raster cleaning, the secondary sputtered ions from the spot area were extracted into the mass spectrometer through a nominal accelerating potential of 4.5 keV. A sample offset voltage of −90 eV (± 15 eV) was used to filter out low-energy background ¹H⁺ desorbed from the raster-cleaned area. Secondary ions were detected by an electron multiplier in pulse-counting mode and were counted using eight cycles of sequential peak switching (background, ¹H⁺, ³⁰Si⁺), following an additional 2 min burn-in to allow secondary ion sputtering to reach a steady state. Intensity ratios, ¹H⁺/³⁰Si⁺, were converted to total H₂O concentrations using calibrations curves constructed from the measurement of standard natural and synthetic basaltic glasses. Two different sets of standards were used: D20–3 (W.G. Melson, personal communication), JED17H (Dixon et al. 1995), and 87s35a#14 (Sisson and Grove 1993b) for glasses with H₂O content ≥ 1.5 wt%, and D20–3, D51–3 and D52–5 (Simons et al. 2002) for glasses with H₂O content ≤ 1.5 wt%. The composition of the basaltic standard glasses is close to the composition of starting materials 82–72f and Bb107, so no correction was applied for matrix effects on 82–72f and Bb107 glasses. Andesitic glass standard 81-T-116 (Sisson and Grove 1993b) gives a higher H₂O value (6.60 wt% instead of 6.17) when analyzed using the basaltic glass calibration curve, and the H₂O concentration for unknown andesitic glass 85–41c#127 was adjusted accordingly. Two to four spots were analyzed on each sample; errors reported in

Table 3 were obtained by combining standard deviation for different analyses on the same sample and errors propagated from the calibration curves.

The H₂O concentration of the glasses was also estimated with the electron microprobe, using two different techniques (Table 3): by analyzing oxygen, and with the “by-difference” method (Devine et al. 1995). Oxygen in glasses was analyzed with the electron microprobe using a LDE1 crystal. Primary calibration was done on a single crystal of gem quality Al₂O₃ carbon-coated together with the samples. H₂O concentrations were then deduced from the oxygen content of the glass. H₂O concentrations were also estimated from the difference between the electron microprobe totals and 100%. For more accurate results, both techniques were calibrated using a set of basaltic and andesitic secondary standards including glasses 81-T-116, 1140mf#18 (Sisson and Grove 1993b), 82–72f#7, #9, #10, #18 (this study), and 0.1 MPa anhydrous glasses. Calibration curves were obtained by plotting H₂O concentrations obtained by difference or by analyzing oxygen against the more accurate H₂O concentrations of the standards (determined by FTIR or SIMS). All the experimental glasses and secondary standards were repolished and carbon-coated at the same time before the analytical session. The use of secondary standards has three different purposes: (1) avoiding matrix effects by using glasses with compositions close to the unknowns, (2) avoiding systematic uncertainties caused by different carbon-coat thicknesses, and (3) taking into account the effect of Fe³⁺ on microprobe totals and oxygen contents, since all experimental and standard glasses have been synthesized under the same oxygen fugacity (NNO). The three analytical techniques are in good agreement (Table 3; Fig. 2), although SIMS values are more accurate.

Experimental results

Liquidus determination

The dry experiments (Table 2) have been used to parameterize the dry olivine-liquidus temperature as a function of pressure. Our high-pressure experimental procedure insures near-anhydrous conditions, as shown by three SIMS analyses on experiment B1042, which contains 0.01 ± 0.05 wt% H_2O . For pressures up to 1.0 GPa, the dry liquidus for 82–72f can be expressed by the equation: $T(^{\circ}C) = 1,267 + 65 \times P(\text{GPa})$. The pressure dependence of $65^{\circ}C/\text{GPa}$ is significantly higher than the $\sim 25^{\circ}C/\text{GPa}$ previously determined by Bartels et al. (1991). Differences can be explained by the presence of H_2O , and the use of different assemblies and thermocouples. Our new preferred value is more consistent with other studies on primitive basalts (e.g., Gust and Perfit 1987; Draper and Johnson 1992). For Bb107, the equation of the dry liquidus is:

$T(^{\circ}C) = 1,275 + 65 \times P(\text{GPa})$. No high-pressure experiment has been performed on 85–41c, since olivine is expected to be the liquidus phase only at low pressures. Assuming that the pressure dependence is similar to that of 82–72f and Bb107, the dry liquidus can be parameterized as: $T(^{\circ}C) = 1,248 + 65 \times P(\text{GPa})$. The uncertainty varies between less than $5^{\circ}C$ at atmospheric pressure up to $10^{\circ}C$ at 1.0 GPa. Below 200 MPa, where most water-saturated experiments have been performed, the uncertainty on the dry liquidus is estimated at $\pm 5^{\circ}C$. The oxygen fugacity in the graphite-capsule high-pressure dry experiments is lower than for all the other experiments that were buffered at NNO. However, variations in oxygen fugacity over this range have little effect on the dry olivine liquidus (e.g., Gust and Perfit 1987).

The water-saturated liquidus for the basaltic composition 82–72f has been bracketed between 0.1 and 1,000 MPa. Assuming an experimental uncertainty of ± 7 and 10 – $15^{\circ}C$ wide brackets, the uncertainty can be estimated to $\pm 14^{\circ}C$ for each bracket. The water-saturated liquidus drops quickly during the first 200 MPa, then levels out at about $1,150^{\circ}C$.

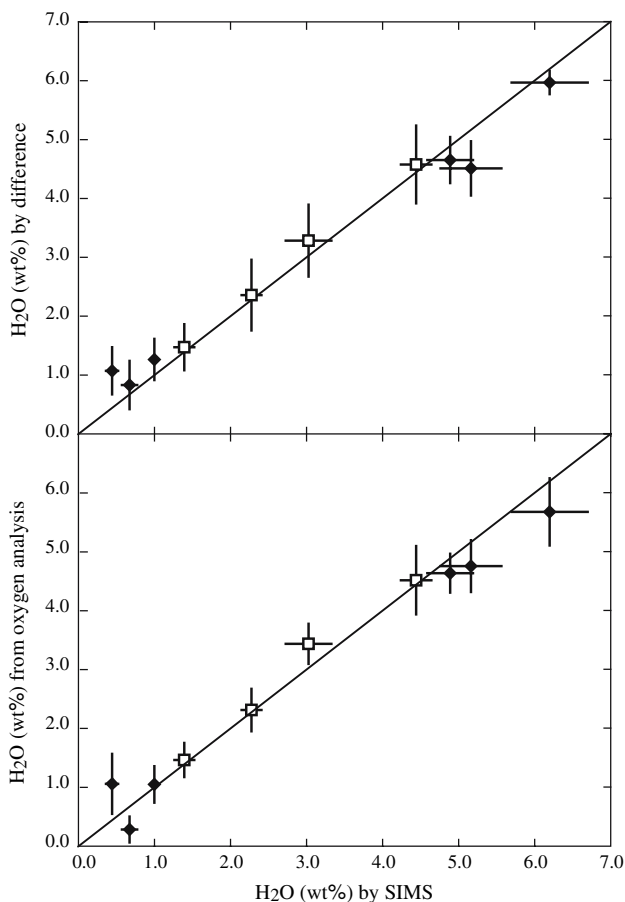


Fig. 2 Comparison of H_2O concentration obtained with the electron microprobe (by difference, and by analyzing oxygen) with H_2O concentrations analyzed by SIMS. *Open symbols* indicate experiments that were used to calibrate the electron microprobe measurements. *Solid symbols* are experiments that were not part of the calibration. *Errors bars* are the 1σ errors as reported in Table 3

Water solubility

H_2O concentrations in 82–72f water-saturated experiments are in excellent agreement with previous solubility experiments on alkali-poor basalts in the range 0–600 MPa (Fig. 3; Table 3; Hamilton et al. 1964; Dixon et al. 1995; Moore et al. 1998). Empirical models (Dixon et al. 1995;

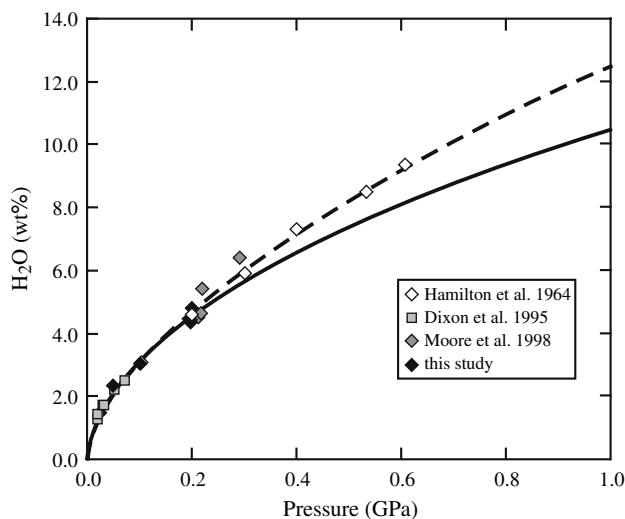


Fig. 3 H_2O solubility in basaltic melts. *Symbols* represent measurements from Hamilton et al. (1964), Dixon et al. (1995), Moore et al. (1998), and this study. *Solid line* and *dashed line* are extrapolated solubilities for basalt 82–72f, from the solubility models of Moore et al. (1998) and Dixon et al. (1995), respectively. For 82–72f, the solubility at 1.0 GPa is estimated between 10.5 and 12.5 wt%

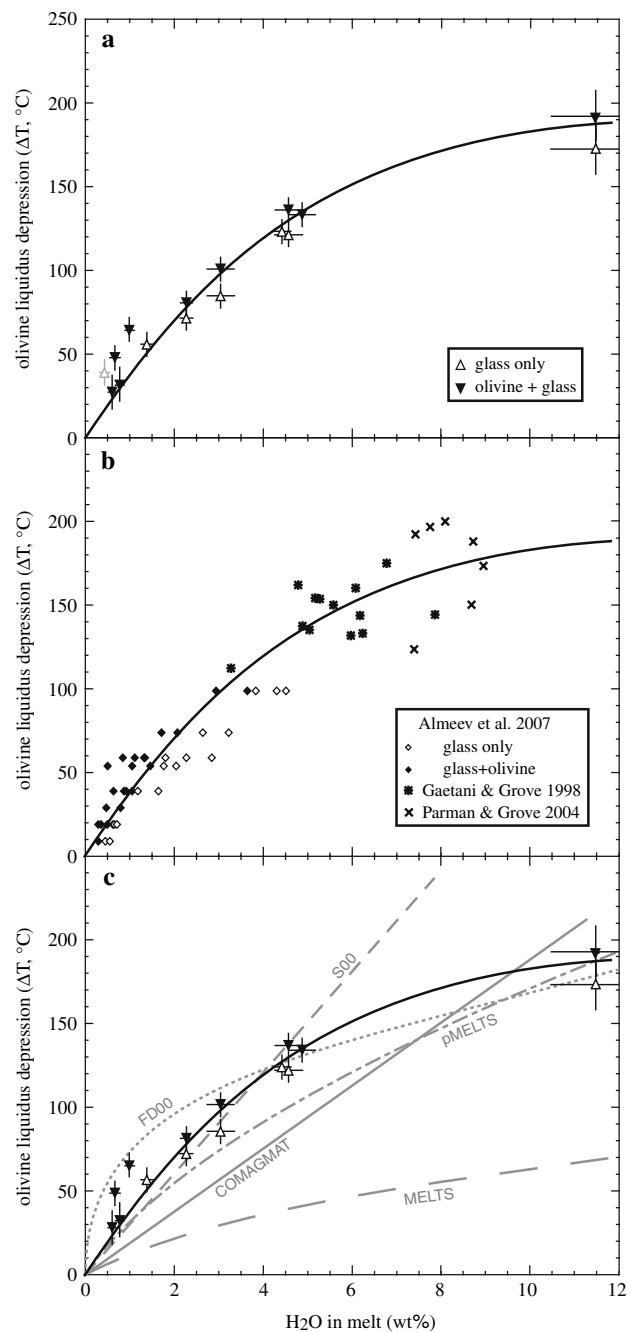
Fig. 4 a Experimental determination of liquidus depression for high-Al basalt 82–72f. For each experiment, the difference between the dry liquidus temperature and the experimental temperature (Table 3) is plotted as a function of H₂O concentration determined by SIMS. When no SIMS measurement was available, concentration for an experiment with the same melt composition and at the same pressure was used. Olivine-free and olivine-bearing experiments bracket the liquidus depression curve. The black curve is a best fit through the data calculated using Eqs (8), (9), and (16), with melt components calculated after Bottinga and Weill (1972). Experiment 82–72f#19, in grey, has been excluded from the model (see text). **b** Comparison between the experimental data, similar experimental data by Almeev et al. (2007), and calculated liquidus depressions for experimental dataset comprising high (>3 wt%) H₂O content experiments (Gaetani and Grove 1998; Parman and Grove 2004). Calculation scheme FDL, as described in Fig. 1. **c** Comparison between experimental data and published models of liquidus depression (see Fig. 1). The black curve is the best fit through the data from Fig. 4a

Moore et al. 1998) extrapolate to a solubility of 10.5–12.5 wt% H₂O at 1.0 GPa (Fig. 3). Water-saturated experiments at 1.0 GPa did not quench to a homogeneous glass, but to a mix of bubbles, glass, and quench crystals, making it impossible to determine H₂O concentrations. In the following analysis, the H₂O content of the 1.0 GPa experiments is assumed to lie between 10.5 and 12.5 wt%, the range spanned by the two empirical models.

Measured water-solubility in the 85–41c andesitic glasses at 200 MPa is significantly higher than the value predicted by the Moore et al. (1998) model (Table 3), but consistent with measurements by Hamilton et al. (1964; ~6 wt% at 200 MPa). This discrepancy might be explained by the strong compositional difference between the andesitic melts used to calibrate Moore's model and 85–41c, which has much higher MgO and FeO and lower Al₂O₃.

Comparison with previous studies

For each near-liquidus hydrous experiment, the difference between the dry liquidus temperature and the experimental temperature has been calculated (Table 3) and plotted as a function of H₂O in the melt (Fig. 4a). Olivine-bearing and olivine-free experiments bracket the liquidus, and thus constrain the amount of liquidus depression. Experiment 82–72f#19 is in disagreement with other experiments, and we choose not to include it in the model. The predicted H₂O concentration from solubility calculations in this 10 MPa experiment is 0.84 wt%, in contrast to the measured 0.44 wt%. Experiment 82–72f#19 could thus have initially been entirely melted, and then moved into the olivine stability field due to H₂O-loss during the experiment. Depending on the timing of H₂O-loss, olivine-nucleation could have been delayed, and the experiment remained melted. The excellent agreement between our data and similar data by Almeev et al. (2007, Fig. 4b) reinforces our choice to exclude experiment 82–72f#19.



The experimental data indicate a stronger effect of water at small water concentration, which progressively weakens at higher water concentration. This non-linear effect is consistent with the model of Falloon and Danyushevsky (2000; Fig. 4c), but of much smaller magnitude. Although its use is not recommended for low-pressure crystallization, the pMELTS thermodynamic model (Ghiorso et al. 2002), gives reasonable results, within 10–30°C of the experimental constraints, and partially accounts for the non-linearity. On the other hand, widely used thermodynamic models such as MELTS (Ghiorso and Sack 1995) and COMAGMAT (Ariskin and Barmina 2004) do not

reproduce the experimental effect of water on the olivine liquidus temperatures.

Falloon and Danyushevsky (2000, Fig. 1) estimated the liquidus depression from the temperature of hydrous experiments, and a dry liquidus temperature calculated from the Ford et al. (1983) geothermometer. This technique will be referred to as FDLT in the following discussion. Successful application of this method requires (1) that the experiments be as close to equilibrium as possible, (2) that the empirical Ford et al. (1983) geothermometer give accurate results over the compositional range investigated, and (3) that the H₂O content of the glass is accurately known. In Fig. 4b, the FDLT treatment has been applied to a selected number of high-H₂O content, high-melt fraction experimental data (Gaetani and Grove 1998; Parman and Grove 2004). Melt compositions in these two studies are high-alumina basalts similar to 82–72f, for which the dry liquidus temperature agrees with the Ford et al. (1983) geothermometer. H₂O contents have been analyzed in all of the experiments, and experiments have been performed at MIT, so there is no interlaboratory bias with our experimental dataset. Calculated liquidus depressions using the FDLT method are in good agreement with the experimental determination on the 82–72f high-alumina basalt (Fig. 4b). Thus the FDLT method can be used on selected experimental datasets. Most of the dispersion on Fig. 1 is probably due to systematic interlaboratory biases or non-applicability of the Ford et al. (1983) thermometer for the investigated composition, or poorly known water concentrations (or even disequilibrium experiments).

Most of our experiments have been performed between 0 and 200 MPa, whereas data by Gaetani and Grove (1998) and Parman and Grove (2004) are in the 1.2–2.0 GPa pressure range. The good agreement between both datasets suggests that pressure has little influence on liquidus depression.

Influence of melt composition

Experiments at 200 MPa indicate that the liquidus depression for alkali-rich melt Bb107 is within error of the liquidus depression for high-alumina basalt 82–72f (Fig. 5) and primitive MORB 140DS1 (Almeev et al. 2007; Fig. 4b). This suggests that for basaltic melts the compositional dependence of the liquidus depression is too small to be resolved by available experimental techniques. As a consequence, the parameterization of liquidus depression for 82–72f can be applied to other basaltic compositions.

Experiments on magnesian andesite 85–41c, however, indicate a much smaller effect of H₂O on liquidus temperatures (Fig. 5). Calculations using the FDLT method also predict smaller liquidus depression for andesitic

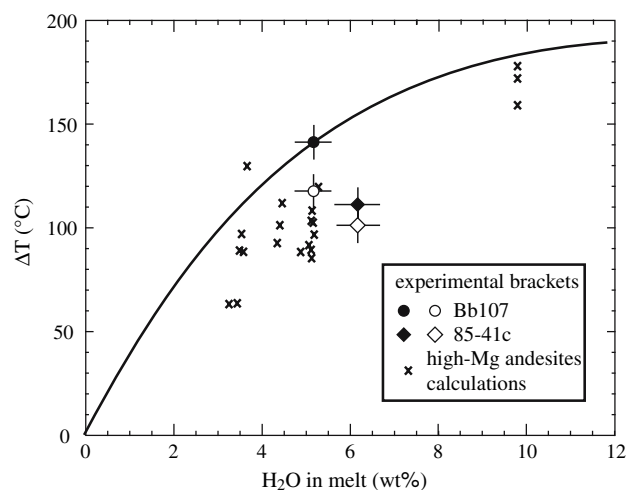


Fig. 5 Effect of composition on liquidus depression. Comparison between high-Al basalt 82–72f (black curve from Fig. 4a), alkali-rich leucite Bb107, and high-Mg andesite 85–41c. Also plotted are calculated liquidus depressions using the FDLT technique for published H₂O-saturated experiments on andesites 85–41c and 1140mf (Grove et al. 1997 and 2003; Krawczynski et al. 2006). For these calculations, results of the Ford et al. (1983) thermometer are corrected for a 30°C offset determined from the dry 0.1 MPa experiments

compositions (Fig. 5). This might be related to the reaction between H₂O and polymerized melt species, producing isolated silica species, and thus stabilizing olivine, a nesosilicate. Lower NBO/T (Table 1) suggests that andesitic melts like 85–41c would be more polymerized than basaltic melts. Since 85–41c has a much higher silica concentration than 82–72f or Bb107, the different effect could also be due to non-ideality in the H₂O–SiO₂ interactions.

Thermodynamic model of liquidus depression

Thermodynamic treatment

The effect of H₂O on the olivine/liquid equilibrium can be expressed in terms of partitioning of olivine end-member components. At equilibrium, the chemical potentials μ of each component i are equal in all phases such that:

$$\mu_i^{\text{olivine}} = \mu_i^{\text{melt}} \quad (1)$$

$$\mu_i^{\text{o,olivine}} + RT \ln(a_i^{\text{olivine}}) = \mu_i^{\text{o,melt}} + RT \ln(a_i^{\text{melt}}) \quad (2)$$

which can be rearranged into:

$$\ln\left(\frac{a_i^{\text{olivine}}}{a_i^{\text{melt}}}\right) = \frac{\Delta G_i^{\text{fusion}}}{RT} \quad (3)$$

This equation can be written for any olivine end-member component, however, only the Mg₂SiO₄ (Fo) and Fe₂SiO₄ components are known with enough accuracy to be useful

for liquidus depression calculations. Since the Mg_2SiO_4 component is the one that shows the largest variations, it will be exclusively used in the model.

Equation (3) can be used to link changes in equilibrium temperature to changes in melt/olivine properties, including the changes caused by the addition of H_2O . The right-hand side of the equation can be written as a function of intensive variables P and T , and experimentally determined thermodynamic properties of pure Mg_2SiO_4 : T_f , the melting point of forsterite at $P = P_o = 10^5$ Pa, $\overline{\Delta C p_{Fo}^f}$, the difference in molar heat capacity between forsterite melt and crystalline forsterite, $\overline{\Delta H_{Fo}^{f,T_f}}$, the molar enthalpy of melting of forsterite at T_f and P_o , and $\overline{\Delta V_{Fo}^f}$, the molar volume change during melting of forsterite:

$$d\left(\frac{\overline{\Delta G_{Fo}^f(T,P)}}{RT}\right) = \left(\frac{\partial\left(\frac{\overline{\Delta G_{Fo}^f(T,P)}}{RT}\right)}{\partial T}\right)_P dT + \left(\frac{\partial\left(\frac{\overline{\Delta G_{Fo}^f(T,P)}}{RT}\right)}{\partial P}\right)_T dP \tag{4}$$

Assuming, as a first approximation, that $\overline{\Delta C p_{Fo}^f} = a + bT$ and that $\overline{\Delta V_{Fo}^f}$ is independent of T and P within the investigated P, T conditions, Eq. (4) leads by substitution to:

$$\frac{\overline{\Delta G_{Fo}^f(T,P)}}{RT} = \int_{T_f}^T \left(\frac{aT_f + \frac{b}{2}T_f^2 - \overline{\Delta H_{Fo}^{f,T_f}}}{RT^2} - \frac{a}{RT} - \frac{b}{2R}\right) dT + \int_{P_o}^P \frac{\overline{\Delta V_{Fo}^f}}{RT} dP \tag{5}$$

These assumptions are justified by the numeric values of $\overline{\Delta C p_{Fo}^f}$ and $\overline{\Delta V_{Fo}^f}$ at 0.1 MPa, and the fact that the compressibilities of forsterite and forsteritic melt are identical within uncertainty under the investigated pressure range (e.g., Ghiorso 2004). Equation (5) can then be integrated to Eq. (6):

$$\frac{\overline{\Delta G_{Fo}^f(T,P)}}{RT} = \frac{1}{R} \left(\overline{\Delta H_{Fo}^{f,T_f}} - aT_f - \frac{b}{2}T_f^2\right) \left(\frac{1}{T} - \frac{1}{T_f}\right) - \frac{a}{R} \ln\left(\frac{T}{T_f}\right) - \frac{b}{2R}(T - T_f) + \frac{\overline{\Delta V_{Fo}^f}(P - P_o)}{RT} \tag{6}$$

Similar expressions have been widely used to build olivine-melt thermometers (e.g., Ford et al. 1983). Equation (3), with the right-hand side substituted by

Eq. (6) can be written for an olivine crystal on the liquidus of a dry melt, at temperature T_d and pressure P . The same equation can be written for an olivine crystal on the liquidus of a H_2O -bearing melt with the same major element composition, at temperature T_w and the same pressure P . Subtracting the two equations gives Eq. (7):

$$\ln\left(\frac{a_{Fo}^{wet\ melt, olivine, T_d}}{a_{Fo}^{dry\ melt, olivine, T_w}}\right) = \frac{1}{R} \left(\overline{\Delta H_{Fo}^{f,T_f}} - aT_f - \frac{b}{2}T_f^2 + \overline{\Delta V_{Fo}^f}(P - P_o)\right) \times \left(\frac{1}{T_d} - \frac{1}{T_w}\right) - \frac{a}{R} \ln\left(\frac{T_d}{T_w}\right) - \frac{b}{2R}(T_d - T_w) \tag{7}$$

The liquidus depression ΔT as defined in the introduction is equal to the difference between T_d and T_w . Experiments on 82–72f demonstrate that the composition of the olivine crystals on the liquidus of a basaltic melt is not influenced by the amount of water dissolved in the melt. For example, the average partition coefficient for Mg (K_{Mg}) for all the experiments is 4.53 ± 0.07 (1σ), within the uncertainty for each individual experiment ($1\sigma = \pm 0.10$) and the Fe–Mg exchange distribution coefficient ($K_D = K_{Fe}/K_{Mg}$) is constant over the range of H_2O contents investigated (Tables 2, 3). The use of partition coefficients rather than raw olivine compositions accounts for the fact that individual experiments are not exactly on the liquidus, and also eliminates the effect of small amounts of Fe loss in a few experiments. The small deviation from ideality in the olivine solid solution can be neglected (Wiser and Wood 1991). Therefore, the activity of olivine on the liquidus of the dry melt is identical to the activity of olivine on the liquidus of the H_2O -bearing melt Eq. (8):

$$\ln\left(\frac{a_{Fo}^{wet\ melt}}{a_{Fo}^{dry\ melt}}\right) = \frac{1}{R} \left(\overline{\Delta H_{Fo}^{f,T_f}} - aT_f - \frac{b}{2}T_f^2 + \overline{\Delta V_{Fo}^f}(P - P_o)\right) \times \left(\frac{1}{T_d} - \frac{1}{T_w}\right) - \frac{a}{R} \ln\left(\frac{T_d}{T_w}\right) - \frac{b}{2R}(T_d - T_w) \tag{8}$$

The right hand-side of Eq. (8) can be calculated from experimentally determined thermodynamic properties, and the liquidus temperatures experimentally determined in this study. These known parameters can then be compared to thermodynamic models of the effect of water on silicate melts, as expressed by the left-hand side of the equation. Or, given a thermodynamic model of the effect of water on silicate melts, ΔT can be calculated from Eq. (8) and compared to experimental determinations.

At 0.1 MPa, pure forsterite melts at $T_f = 2,163$ K (Robie and Hemingway 1995). The enthalpy of fusion

$\overline{\Delta H_{\text{Fo}}^{f,T_i}}$ has been determined as $142 \pm 14 \text{ kJ mol}^{-1}$ from calorimetric measurements (Richet et al. 1993). $\overline{\Delta Cp_{\text{Fo}}^f}$ can be calculated from the heat capacity of crystalline Mg_2SiO_4 (Gillet et al. 1991), and the temperature-independent heat capacity of liquid Mg_2SiO_4 ($252 \text{ J mol}^{-1} \text{ K}^{-1}$, extrapolated from the model of Richet and Bottinga 1985). $\overline{\Delta Cp_{\text{Fo}}^f}$ varies linearly over the investigated temperature range according to the equation $\overline{\Delta Cp_{\text{Fo}}^f} = a + bT$, with $a = 100 \text{ J mol}^{-1} \text{ K}^{-1}$, and $b = -0.0242 \text{ J mol}^{-1} \text{ K}^{-2}$. $\overline{\Delta V_{\text{Fo}}^f} = 3.25 \text{ cm}^3 \text{ mol}^{-1}$ has been calculated from the Clapeyron slope of the Mg_2SiO_4 melting reaction (David and England 1964) and is in general agreement with a $3\text{--}7 \text{ cm}^3 \text{ mol}^{-1}$ estimate made from the molar volumes of solid Mg_2SiO_4 (Robie and Hemingway 1995) and liquid Mg_2SiO_4 (extrapolated from the model of Courtial and Dingwell 1999).

Non-ideal behavior of H_2O in silicate melts

The activity of the Mg_2SiO_4 component in the melt can be calculated from the concentrations of MgO and SiO_2 :

$$\begin{aligned} \frac{a_{\text{wet melt}}^{\text{Fo}}}{a_{\text{dry melt}}^{\text{Fo}}} &= \frac{\left(X_{\text{wet}}^{\text{MgO}}\right)^2 X_{\text{wet}}^{\text{SiO}_2} \left(\gamma_{\text{wet}}^{\text{MgO}}\right)^2 \gamma_{\text{wet}}^{\text{SiO}_2}}{\left(X_{\text{dry}}^{\text{MgO}}\right)^2 X_{\text{dry}}^{\text{SiO}_2} \left(\gamma_{\text{dry}}^{\text{MgO}}\right)^2 \gamma_{\text{dry}}^{\text{SiO}_2}} \\ &= \left(1 - X_{\text{wet}}^{\text{H}_2\text{O}}\right)^3 \frac{\left(\gamma_{\text{wet}}^{\text{MgO}}\right)^2 \gamma_{\text{wet}}^{\text{SiO}_2}}{\left(\gamma_{\text{dry}}^{\text{MgO}}\right)^2 \gamma_{\text{dry}}^{\text{SiO}_2}} \end{aligned} \quad (9)$$

The first part of Eq. (9) is the simple dilution effect caused by the addition of H_2O to the melt. The second part quantifies the non-ideality of H_2O solution, either due to modification of the melt structure or configurational excess energy of mixing. In a first step we assume that this effect is negligible, i.e. that the addition of water follows an ideal solution model. Although the predicted effect is close to the experimental results (Fig. 6), this ideal solution model fails to explain the non-linearity of the liquidus depression.

The effect of H_2O on the melt structure has been successfully quantified in simple systems (albite- H_2O , diopside- H_2O , quartz- H_2O) by Silver and Stolper (1985). In their model (see also Toop and Samis 1962), hydrous silicate melts are modeled as mixtures of three quasi-chemical oxygen species: oxygen atoms O, hydroxyl groups OH and water molecules H_2O . Water molecules H_2O react with the oxygen atoms to produce hydroxyl groups through the following homogeneous equilibria (Silver and Stolper 1985):

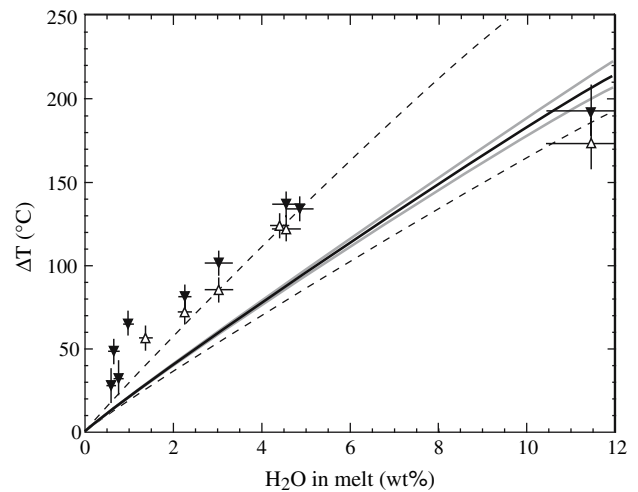


Fig. 6 Thermodynamic models of olivine liquidus depression assuming ideal mixing of H_2O in silicate melts (activity = concentration). The model represented by the *black line* uses the thermodynamic values described in the text. The two *grey lines* show the influence of the molar volume change ΔV_{Fo} , varying between 0 (lower line) and $7 \text{ cm}^3 \text{ mol}^{-1}$. The dashed lines delimit the range of models allowed by the uncertainties on enthalpy and heat capacity determination. Experimental data are from Fig. 4a. T_w is calculated using Eqs. (8) and (9), $\Delta T = T_d - T_w$. Melt fractions are derived using the calculation scheme of Bottinga and Weill (1972)

This equilibrium is controlled by the dissociation constant:

$$K_1 = \frac{\left(a_{\text{melt}}^{\text{OH}}\right)^2}{\left(a_{\text{melt}}^{\text{O}}\right)\left(a_{\text{melt}}^{\text{H}_2\text{O}}\right)} \quad (11)$$

Following the model of Silver and Stolper (1985), we assume ideal mixing (i.e., activity coefficients equals to 1) and calculate the concentration of oxygen atoms $X_{\text{melt}}^{\text{O}}$ as a function of water concentration and the dissociation constant K_1 . The activity of the Mg_2SiO_4 component in the silicate melt is then defined by:

$$a_{\text{wet melt}}^{\text{Fo}} = a_{\text{dry melt}}^{\text{Fo}} \left(X_{\text{wet melt}}^{\text{O}}\right)^4 \quad (12)$$

Equation (12) can then be plugged into Eq. (8) to calculate the amount of liquidus depression. This model assigns a special role to water, which is not considered as a regular component of the melt but only reacts with the oxygen atoms, decreasing the activities of the other components. This quasi-ideal mixing model gives results extremely similar to the previous ideal model, and does not explain the non-linearity of the experimental results (Fig. 7). A very similar approach based on H_2O speciation has been developed by Maksimov (2003). As with the model presented in Fig. 7, the calculated liquidus depression is in general qualitative agreement with our experimental data, but cannot give a quantitative explanation. In particular, it

fails to account for the strong temperature—lowering effect at low water concentration, and the leveling out observed at high water concentration. Maksimov (2003) shows that there is a good agreement between experiments and model predictions for the water-saturated basalt liquidus. His model indeed agrees with the old and poorly constrained data—relative to modern experimental standards—of Yoder and Tilley (1962), but does not fit with our experimental determination of the water-saturated basalt liquidus. It is possible that in the work by Silver and Stolper (1985), the thermodynamics of the relatively simple silicate melts (NaAlSi₃O₈, CaMgSi₂O₆, SiO₂) can be accounted for by a limited number of network-former species, and the single depolymerizing reaction Eq. (10). In more complex silicate melts, however, the presence of different polymer species, and interaction between H₂O and other network modifiers like Na₂O, may require a more complicated set of speciation reactions. Alternatively, non-ideal terms linked to the configurational entropy of mixing could preclude the use of a simple thermodynamic parameterization of water solution. It is also possible that there are discrepancies between dry liquidus determinations and H₂O-saturated melting experiments. For example the liquidus of pure albite has been difficult to determine accurately (Bohlen et al. 1982). In our analysis the low-H₂O content experiments at low pressure strongly influence the model.

Another approach to this problem, similar to the one adopted by Nicholls (1980) is to use Margules parameters to account for the non-ideality of H₂O dissolution in silicate melt. We assume that upon dissolution of H₂O, most of the non-ideality is due to interactions between H₂O and

SiO₂ and that interactions between H₂O and MgO are ideal ($\gamma_{\text{MgO}}^{\text{wet}} = \gamma_{\text{MgO}}^{\text{dry}}$, see Gaetani and Grove 1998). The activity coefficient for SiO₂ can be expressed as:

$$RT_d \ln (\gamma_{\text{SiO}_2}^{\text{dry}}) = \sum_j W_{\text{SiO}_2,j} (X_j^{\text{dry}})^2 \tag{13}$$

$$\begin{aligned} RT_w \ln (\gamma_{\text{SiO}_2}^{\text{wet}}) &= \sum_j W_{\text{SiO}_2,j} (X_j^{\text{wet}})^2 + W_{\text{SiO}_2,\text{H}_2\text{O}} (X_{\text{H}_2\text{O}})^2 \\ &= (1 - X_{\text{H}_2\text{O}})^2 \sum_j W_{\text{SiO}_2,j} (X_j^{\text{dry}})^2 + W_{\text{SiO}_2,\text{H}_2\text{O}} (X_{\text{H}_2\text{O}})^2 \end{aligned} \tag{14}$$

In these equations, *j* stands for melt components other than SiO₂ and H₂O,

$$\sum = \sum_j W_{\text{SiO}_2,j} (X_j^{\text{d}})^2 \tag{15}$$

takes into account the interactions between the SiO₂ component and other melt components in the dry melt, and $W = W_{\text{SiO}_2,\text{H}_2\text{O}}$ takes into account the interaction between H₂O and SiO₂ components. It is assumed as a first order-approximation, that the interactions between melt components are independent of each other. Equations (13) and (14) can be rearranged to:

$$\ln \left(\frac{\gamma_{\text{SiO}_2}^{\text{w}}}{\gamma_{\text{SiO}_2}^{\text{d}}} \right) = \frac{(W + \sum)}{RT_w} (X_{\text{H}_2\text{O}})^2 - \frac{2\sum}{RT_w} X_{\text{H}_2\text{O}} + \frac{\sum}{R} \left(\frac{1}{T_w} - \frac{1}{T_d} \right) \tag{16}$$

This quadratic equation can be solved for *W* and \sum using the experimental data, and gives $\sum = 28.9 \text{ kJ mol}^{-1}$ for the basaltic melt 82–72f, and $W = 129 \text{ kJ mol}^{-1}$. Using these two values, it is possible to get an excellent fit of the experimental data from Eqs. (8) and (16) (Fig. 4a). The values obtained here for *W* and \sum are highly dependent on the values of the thermodynamic properties (enthalpy, heat capacity) and on the choice of melt components, and cannot easily be transposed to other models (like pMELTS).

Influence of pressure and melt composition

The thermodynamic model can be used together with experimental data to investigate the effect of pressure and melt composition on the olivine/melt equilibrium. Comparison between our polybaric experimental data, the 200 MPa experiments of Almeev et al. (2007), and liquidus depression estimates using the FDL method (Fig. 4b), suggest that pressure has little influence on liquidus depression. The effect of pressure increases with H₂O

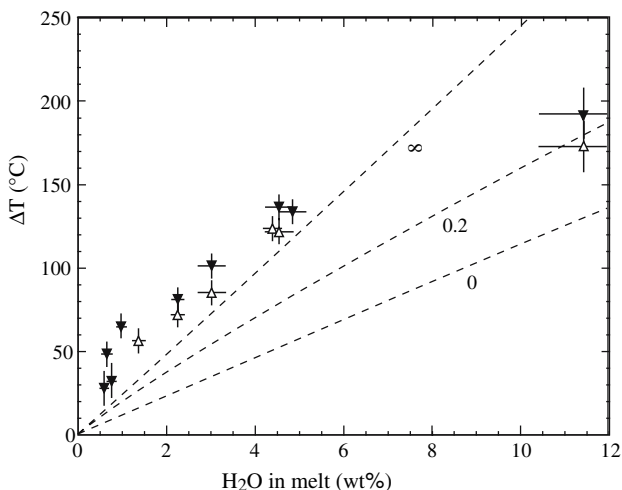


Fig. 7 Thermodynamic models of olivine liquidus depression using ideal mixing of quasi-chemical oxygen species (Silver and Stolper 1985; Toop and Samis 1962). Numbers on the curves are values of the *K*₁ equilibrium constant. Experimental data are from Fig. 4a. Calculation uses Eqs. (8) and (12) and equation 5.3 of Silver and Stolper (1985)

concentration. However, for pressures between 0 and 2.0 GPa, the thermodynamic model predicts only a 3.4°C variation at 5.0 wt% H₂O. Changing the value of $\overline{\Delta V}_{\text{Fo}}^f$ within the experimentally permitted range (3–7 cm³ mol⁻¹) does not significantly change the effect. The effect of pressure on liquidus depression can thus be neglected.

Experiments indicate that, within uncertainty, the liquidus depression is the same for high-alumina basalt 82–72f, alkali-rich leucite Bb107, and the primitive tholeiitic basalt studied by Almeev et al. (2007, Fig. 4b, 5). This suggests that for primitive basaltic compositions, the effect of melt composition is negligible and the liquidus depression can thus be approximated by the pressure- and composition-independent power series:

$$\Delta T \text{ (}^\circ\text{C)} = 40.4 \left(C_{\text{H}_2\text{O}}^{\text{melt}} \right) - 2.97 \left(C_{\text{H}_2\text{O}}^{\text{melt}} \right)^2 + 0.0761 \left(C_{\text{H}_2\text{O}}^{\text{melt}} \right)^3 \quad (17)$$

where $C_{\text{H}_2\text{O}}^{\text{melt}}$ is in weight percent. The linear approximation is valid within 5°C up to 1.3 wt% H₂O and can thus be used in models pertaining to the crystallization of MORB. For higher H₂O contents, the second order polynomial can be used up to 4.0 wt% H₂O, and the third order polynomial stays within 1°C of the thermodynamic model over the entire experimental range.

Equation (17) is expected to be valid for most olivine-saturated magmatic compositions, with the exception of silica-rich compositions similar to 85–41c, which includes very low degree mantle melts (Baker et al. 1995; Hirose 1997), and some silica-rich primitive subduction-zone magmas (high-Mg andesites, boninites). For composition 85–41c, experimental data suggest that the effect of H₂O is smaller than for a basaltic melt, and closer to linearity (Fig. 5). This could be qualitatively explained by two competitive effects of H₂O in silicate melts: (1) H₂O interacts with Si–O–M bonds (where M stands for any network-modifier cation, including Mg²⁺), producing Si–OH species, and thus reducing the stability of crystalline silicate phases, including olivine; (2) H₂O also breaks Si–O–Si bonds in polymerized species, reducing the overall degree of polymerization of the melt, and thus favoring the crystallization of non-polymerized minerals like olivine. This second effect is responsible for the enhanced stability of olivine relative to other silicate phases in hydrous melts (e.g., Kushiro 1969), and should be more important for the most polymerized melts, like 85–41c (NBO/T = 0.6).

Conclusions

For primitive basaltic melts, the influence of H₂O on liquidus temperature appears to be independent of

composition, but there is a compositional effect for high-SiO₂ liquids. The non-linearity of the liquidus depression as a function of H₂O content cannot be explained by an ideal solution model, nor by a speciation model involving ideal mixing of oxygen quasi-chemical species as developed in simple systems like albite–H₂O or diopside–H₂O (Silver and Stolper 1985). A better fit is obtained with a non-ideal solution model that treats the effect of H₂O addition as a positive excess free energy. This indicates that incorporation of H₂O in silicate melts is non-ideal, and involves interaction between H₂O and other melt components. Experiments and thermodynamic calculation also indicates that there is no pressure effect on the liquidus depression, and that it levels out at high H₂O contents (>10 wt%). This may have implications for the shape of the liquidus of silicate melts at high pressure, as well as for the P/T slope of the wet solidus in subducted basalts and mantle lherzolites. Finally, since the composition of liquidus olivine does not change with H₂O content of the melt, liquidus temperatures of hydrous magmas can be determined by using a dry olivine–melt thermometer, and then correcting for the effect of H₂O using Eq. (17).

Acknowledgments Technical assistance provided by N. Shimizu with the ion microprobe is greatly appreciated. Critical comments by two anonymous reviewers greatly improved the manuscript. This research was supported by grants EAR0440172, EAR0538179 and EAR0440045 from the National Science Foundation.

References

- Almeev R, Holtz F, Koepke J, Parat F, Botcharnikov RE (2007) The effect of H₂O on olivine crystallization in MORB: experimental calibration at 200 MPa. *Am Mineral* 92:670–674
- Anderson ATJ (1979) Water in some hypersthenic magmas. *J Geol* 87:509–531
- Ariskin AA, Barmina GS (2004) COMAGMAT: development of a magma crystallization model and its petrological implications. *Geochem Int* 42(Suppl 1):S1–S157
- Armstrong JT (1995) CITZAF—a package of correction programs for the quantitative electron microbeam X-ray analysis of thick polished materials, thin-films, and particles. *Microbeam Anal* 4:177–200
- Asimow PD, Langmuir CH (2003) The importance of water to oceanic mantle melting regimes. *Nature* 421:815–820
- Baker MB, Grove TL, Price RC (1994) Primitive basalts and andesites from the Mt. Shasta region, N. California: products of varying melt fraction and water content. *Contrib Mineral Petrol* 118:111–129
- Baker MB, Hirschmann MM, Ghiorso MS, Stolper EM (1995) Compositions of near-solidus peridotite melts from experiments and thermodynamic calculations. *Nature* 375:308–311
- Bartels KS, Kinzler RJ, Grove TL (1991) High pressure phase relations of primitive high-alumina basalts from Medicine Lake volcano, northern California. *Contrib Mineral Petrol* 108:253–270
- Bohlen SR, Boettcher AL, Wall VJ (1982) The system albite–H₂O–CO₂: a model for melting and activities of water at high pressures. *Am Mineral* 67:451–462

- Bottinga Y, Weill DF (1972) The viscosity of magmatic silicate liquids: a model for calculation. *Am J Sci* 272:438–475
- Boyd FR, England JL (1960) Apparatus for phase equilibrium measurements of pressures up to 50 kbars and temperatures up to 1750°C. *J Geophys Res* 65:741–748
- Courtial P, Dingwell DB (1999) Densities of melts in the CaO–MgO–Al₂O₃–SiO₂ system. *Am Mineral* 84:465–476
- Danyushevsky LV (2001) The effect of small amounts of H₂O on crystallisation of mid-ocean ridge and backarc basin magmas. *J Volcanol Geotherm Res* 110:265–280
- Danyushevsky LV, Falloon TJ, Sobolev AV, Crawford AJ, Carroll M, Price RC (1993) The H₂O content of basalt glasses from southwest Pacific back-arc basins. *Earth Planet Sci Lett* 117:347–362
- David BTC, England JL (1964) The melting of forsterite up to 50 kilobars. *J Geophys Res* 69:1113–1116
- Devine JD, Gardner JE, Brack HP, Layne GD, Rutherford MJ (1995) Comparison of microanalytical methods for estimating H₂O contents of silicic volcanic glasses. *Am Mineral* 80:319–328
- Dixon JE, Clague DA, Wallace P, Poreda R (1997) Volatiles in alkalic basalts from the North Arch volcanic field, Hawaii: extensive degassing of deep submarine-erupted alkalic series lavas. *J Petrol* 38:911–939
- Dixon JE, Stolper EM, Holloway JR (1995) An experimental study of water and carbon dioxide solubilities in mid-ocean ridge basaltic liquids. Part I: calibration and solubility models. *J Petrol* 36:1607–1631
- Donnelly-Nolan JM, Champion DE, Grove TL, Baker MB, Taggart JE, Bruggman PE (1991) The Giant Crater lava-field—geology and geochemistry of a compositionally zoned, high-alumina basalt to basaltic andesite eruption at Medicine Lake Volcano, California. *J Geophys Res* 96:21843–21863
- Draper D, Johnson A (1992) Anhydrous PT phase relations of an Aleutian high-MgO basalt: an investigation of the role of olivine-liquid reaction in the generation of arc high-alumina basalts. *Contrib Mineral Petrol* 112:501–519
- Falloon TJ, Danyushevsky LV (2000) Melting of refractory mantle at 1.5, 2 and 2.5 GPa under anhydrous and H₂O-undersaturated conditions: implications for the petrogenesis of high-Ca boninites and the influence of subduction components on mantle melting. *J Petrol* 41:257–283
- Ford CE, Russell DG, Craven JA, Fisk MR (1983) Olivine-liquid equilibria: temperature, pressure and composition dependence of the crystal/liquid cation partition coefficients for Mg, Fe²⁺, Ca and Mn. *J Petrol* 24:256–265
- Gaetani GA, Grove TL (1998) The influence of water on melting of mantle peridotite. *Contrib Mineral Petrol* 131:323–346
- Ghiorso MS (2004) An equation of state for silicate melts. III. Analysis of stoichiometric liquids at elevated pressure: shock compression data, molecular dynamics simulations and mineral fusion curves. *Am J Sci* 304(8–9):752–810
- Ghiorso MS, Hirschmann MM, Reiners PW, Kress VC (2002) The pMELTS: a revision of MELTS for improved calculation of phase relations and major element partitioning related to partial melting of the mantle to 3 GPa. *Geochem Geophys Geosyst* 3. doi:10.1029/2001GC000217
- Ghiorso MS, Sack RO (1995) Chemical mass-transfer in magmatic processes 4. A revised and internally consistent thermodynamic model for the interpolation of solid-liquid equilibria in magmatic systems at elevated temperatures and pressures. *Contrib Mineral Petrol* 119:197–212
- Gillet P, Richet P, Guyot F, Fiquet G (1991) High-temperature thermodynamic properties of forsterite. *J Geophys Res* 96:11805–11816
- Green DH, Falloon TJ, Eggins SM, Yaxley GM (2001) Primary magmas and mantle temperatures. *Eur J Mineral* 13:437–451
- Grove TL (1981) Use of PtFe to eliminate the iron-loss problem in 1 atmosphere gas mixing experiments: theoretical and practical considerations. *Contrib Mineral Petrol* 78:298–304
- Grove TL, Baker MB (1984) Phase equilibrium controls on tholeiitic versus calc-alkaline differentiation trends. *J Geophys Res* 89:3253–3274
- Grove TL, Baker MB, Price RC, Parman SW, Elkins-Tanton LT, Chatterjee N, Müntener O (2005) Magnesian andesite and dacite lavas from Mt. Shasta, northern California: products of fractional crystallization of H₂O-rich mantle melts. *Contrib Mineral Petrol* 148:542–565
- Grove TL, Chatterjee N, Parman SW, Médard E (2006) The influence of H₂O on mantle wedge melting. *Earth Planet Sci Lett* 249: 74–89
- Grove TL, Donnelly-Nolan JM, Housh T (1997) Magmatic processes that generated the rhyolite of Glass Mountain, Medicine Lake Volcano, N California. *Contrib Mineral Petrol* 127:205–223
- Grove TL, Elkins-Tanton LT, Parman SW, Chatterjee N, Müntener O, Gaetani GA (2003) Fractional crystallization and mantle-melting controls on calc-alkaline differentiation trends. *Contrib Mineral Petrol* 145:515–533
- Gust DA, Perfit MR (1987) Phase relations of a high-Mg basalt from the Aleutian Island Arc: implications for primary island arc basalts and high-Al basalts. *Contrib Mineral Petrol* 97:7–18
- Hamilton DL, Burnham CW, Osborn EF (1964) The solubility of water and effects of oxygen fugacity on crystallization in mafic magmas. *J Petrol* 5:21–39
- Hays JF (1966) Lime-alumina-silica. *Carnegie Inst Wash Yearb* 65:234–239
- Hirose K (1997) Melting experiments on Iherzolite KLB-1 under hydrous conditions and generation of high-magnesian andesitic melts. *Geology* 25:42–44
- Holbig ES, Grove TL (2007) Mantle melting beneath the Tibetan Plateau: experimental constraints on ultra-potassic magmatism. *J Geophys Res* (in press)
- Kägi R, Müntener O, Ulmer P, Ottolini L (2005) Piston-cylinder experiments on H₂O undersaturated Fe-bearing systems: an experimental setup approaching fO₂ conditions of natural calc-alkaline magmas. *Am Mineral* 90:708–717
- Krawczynski MJ, Grove TL, Médard E, Barr JA, Till CB, Behrens H (2006) The fate of wet mantle melts: fractionation crystallization processes preserved in magmatic inclusions, Mt. Shasta CA. *Eos Trans. AGU, Fall Meet. Suppl.*, Abstract V14B-06
- Kushiro I (1969) The system forsterite-diopside-silica with and without water at high pressures. *Am J Sci* 267:269–294
- Langmuir CH, Bézous A, Escrig S, Parman SW (2006) Chemical systematics and hydrous melting of the mantle in back-arc basins. In: *Back-arc spreading systems: geological, biological, chemical, and physical interactions*. Geophysical Monograph 166, American Geophysical Union pp 87–146
- Laporte D, Toplis MJ, Seyler M, Devidal J-L (2004) A new experimental technique for extracting liquids from peridotite at very low degrees of melting: application to partial melting of depleted peridotite. *Contrib Mineral Petrol* 146:463–484
- Maksimov AP (2003) Effect of water on the melting curves of minerals: the olivine-melt equilibrium. *Geochem Int* 41:947–958
- Médard E, Schmidt MW, Schiano P, Ottolini L (2006) Melting of amphibole-bearing wehrlites: an experimental study on the origin of ultra-calcic nepheline-normative melts. *J Petrol* 47:481–504
- Michael PJ, Chase RL (1987) The influence of primary magma composition, H₂O and pressure on mid-ocean ridge basalt differentiation. *Contrib Mineral Petrol* 96:245–263
- Moore G, Vennemann T, Charmichael ISE (1998) An empirical model for the solubility of H₂O in magmas to 3 kilobars. *Am Mineral* 83:36–42

- Mysen BO, Boettcher AL (1975) Melting of a hydrous mantle: I. Phase relations of natural peridotite at high pressures and temperatures with controlled activities of water, carbon dioxide, and hydrogen. *J Petrol* 16:520–548
- Nicholls J (1980) A simple thermodynamic model for estimating the solubility of H₂O in magmas. *Contrib Mineral Petrol* 74:211–220
- Parman SW, Grove TL (2004) Harzburgite melting with and without H₂O: experimental data and predictive modeling. *J Geophys Res* 109:B02201. doi:10.1029/2003JB002566
- Pichavant M, Mysen BO, Macdonald R (2002) Source and H₂O content of high-MgO magmas in island arc settings: an experimental study of a primitive calc-alkaline basalt from St. Vincent, Lesser Antilles arc. *Geochim Cosmochim Acta* 66:2193–2209
- Putirka K (2005) Mantle potential temperatures at Hawaii, Iceland, and the mid-ocean ridge system, as inferred from olivine phenocrysts: evidence for thermally-driven mantle plumes. *Geochem Geophys Geosyst* 6:Q05L08. doi:10.1029/2005GC000915
- Richet P, Bottinga Y (1985) Heat capacity of aluminum-free liquid silicates. *Geochim Cosmochim Acta* 49:471–486
- Richet P, Leclerc F, Benoist L (1993) Melting of forsterite and spinel with implications for the glass transition of Mg₂SiO₄ liquid. *Geophys Res Lett* 20:1675–1678
- Robie RA, Hemingway BS (1995) Thermodynamic properties of minerals and related substances at 298.15 K and 1 bar (10⁵ Pa) pressure and higher temperatures. USGS Bulletin 2131
- Roeder PL, Emslie RF (1970) Olivine-liquid equilibrium. *Contrib Mineral Petrol* 19:275–289
- Silver L, Stolper EM (1985) A thermodynamic model for hydrous silicate melts. *J Geol* 93:161–178
- Simons K, Dixon JE, Schilling J-G, Kingsley R, Poreda R (2002) Volatiles in basaltic glasses from the Easter-Sala y Gomez seamount chain and Easter microplate: implications for geochemical cycling of volatile elements. *Geochem Geophys Geosyst* 3:1039. doi:10.1029/2001GC000173
- Sisson TW, Grove TL (1993a) Experimental investigations of the role of H₂O in calc-alkaline differentiation and subduction zone magmatism. *Contrib Mineral Petrol* 113:143–166
- Sisson TW, Grove TL (1993b) Temperatures and H₂O contents of low-MgO high-alumina basalts. *Contrib Mineral Petrol* 113:167–184
- Sisson TW, Layne GD (1993) H₂O in basalt and andesite glass inclusions from four subduction-related volcanoes. *Earth Planet Sci Lett* 117:619–635
- Sobolev AV, Chaussidon M (1996) H₂O concentrations in primary melts from supra-subduction zones and mid-ocean ridges: implications for H₂O storage and recycling in the mantle. *Earth Planet Sci Lett* 137:45–55
- Spilliaert N, Allard P, Métrich N, Sobolev AV (2006) Melt inclusion record of the conditions of ascent, degassing and extrusion of volatile-rich alkali basalt during the powerful 2002 flank eruption of Mount Etna (Italy). *J Geophys Res* 111:B04203. doi:10.1029/2005JB003934
- Stolper EM, Newman S (1994) The role of water in the petrogenesis of Mariana trough magmas. *Earth Planet Sci Lett* 121:293–325
- Sugawara T (2000) Empirical relationships between temperature, pressure, and MgO content in olivine and pyroxene saturated liquid. *J Geophys Res* 106:8457–8472
- Toop GW, Samis CS (1962) Activities of ions in silicate melts. *Trans Metall Soc AIME* 224:878–887
- Turner S, Arnaud N, Liu J, Hawkesworth NRC, Harris N, Kelley S, VanCalsteren P, Deng W (1996) Post-collision, shoshonitic volcanism on the Tibetan plateau: implications for convective thinning of the lithosphere and the source of ocean island basalts. *J Petrol* 37:45–71
- Watson EB, Wark DA, Price JD, van Orman JA (2002) Mapping the thermal structure of solid-media pressure assemblies. *Contrib Mineral Petrol* 142:640–652
- Wiser NM, Wood BJ (1991) Experimental determination of activities in Fe-Mg olivine at 1400 K. *Contrib Mineral Petrol* 108(1):146–153
- Workman RK, Hart SR (2005) Major and trace element composition of the depleted MORB mantle (DMM). *Earth Planet Sci Lett* 231:53–72
- Yoder HSJ, Tilley CE (1962) Origin of basalt magmas: an experimental study of natural and synthetic rock systems. *J Petrol* 3:342–532